

Phase Transformation of Materials

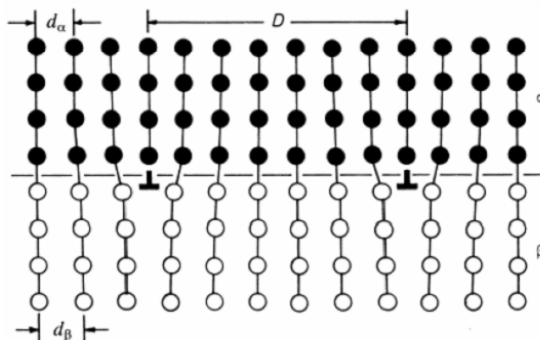
Nong-Moon Hwang

Nov. 6, 2008



If coherency strain energy is too large. → misfit dislocations

How would you define misfit in terms of d_α and d_β ?



$$\delta = \frac{d_\beta - d_\alpha}{d_\alpha}$$

$$D = \frac{b}{\delta}$$

δ : misfit (disregistry)

Fig. 3.35 A semicoherent interface. The misfit parallel to the interface is accommodated by a series of edge dislocations.



2) Semicoherent Interfaces

$\gamma(\text{semicoherent}) = \gamma_{ch} + \gamma_{st}$ $\gamma_{st} \rightarrow$ due to structural distortions caused by the misfit dislocations
 $\rightarrow 200 \sim 500 \text{ mJm}^{-2}$

$\gamma_{st} \propto \delta$ for small $\delta \rightarrow$ It levels out when $\delta \cong 0.25$.

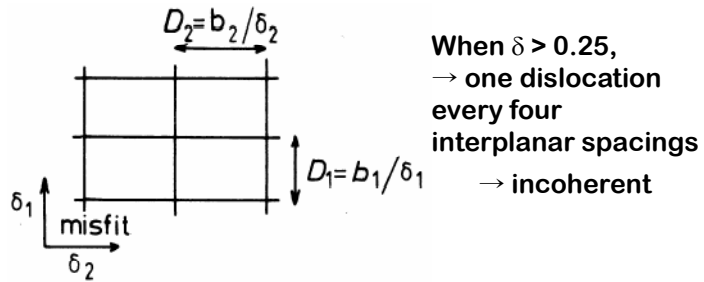


Fig. 3.36 Misfit in two directions (δ_1 and δ_2) can be accommodated by a cross-grid of edge dislocations with spacings $D_1 = b_1/\delta_1$ and $D_2 = b_2/\delta_2$



3) Incoherent Interfaces

$\gamma(\text{incoherent}) \approx 500 \sim 1000 \text{ mJm}^{-2}$

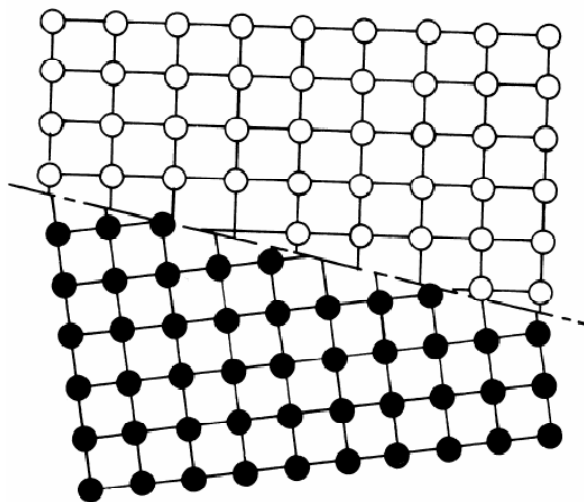


Fig. 3.37 An incoherent interface.



4) Complex Semicoherent Interfaces

If bcc α is precipitated from fcc γ , which interface is expected?

Which orientation would make the lowest interface energy?

Nishiyama-Wasserman (N-W) Relationship

$$(110)_{bcc} // (111)_{fcc}, [001]_{bcc} // [\bar{1}01]_{fcc}$$

Kurdjumov-Sachs (K-S) Relationships

$$(110)_{bcc} // (111)_{fcc}, [1\bar{1}1]_{bcc} // [0\bar{1}1]_{fcc}$$



4) Complex Semicoherent Interfaces

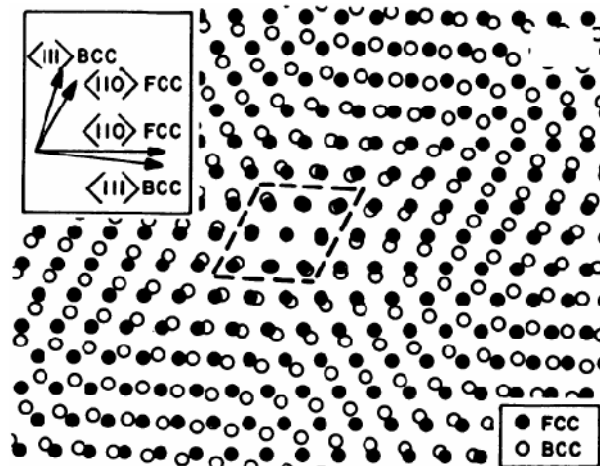


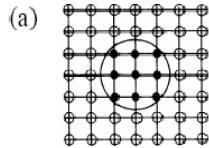
Fig. 3.38 Atomic matching across a $(111)_{fcc}/(110)_{bcc}$ interface bearing the NW orientation relationship for lattice parameters closely corresponding to the case of fcc and bcc iron. (M.G. Hall *et al.*, *Surface Science*, 31 (1972)257).



3.4.2 Second-Phase Shape: Interfacial Energy Effects

How is the second-phase shape determined? → Interfacial and Strain E.
→ Growth Kinetics

$$\sum A_i \gamma_i = \text{minimum}$$



GP (Guinier- Preston) Zone
in Al - Ag Alloys

$$\varepsilon_a = \frac{r_A - r_B}{r_A} = 0.7\%$$

→ negligible contribution
to the total free energy

Fully Coherent Precipitate

→ spherical

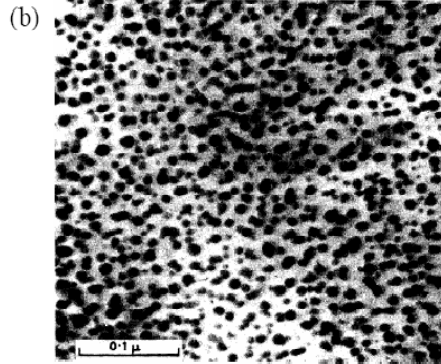


Fig. 3.39 (a) A zone with no misfit (○ Al, ● Ag, for example), (b) Electron micrograph of Ag-rich zones in an Al-4 atomic % Ag alloy ($\times 300\,000$). (After R.B. Nicholson, G. Thomas and J. Nutting, *Journal of the Institute of Metals*, 87 (1958-1959) 431.)

Partially Coherent Precipitates

It should be noted that
the observed ppt shape
is a growth shape,
not an equilibrium shape.

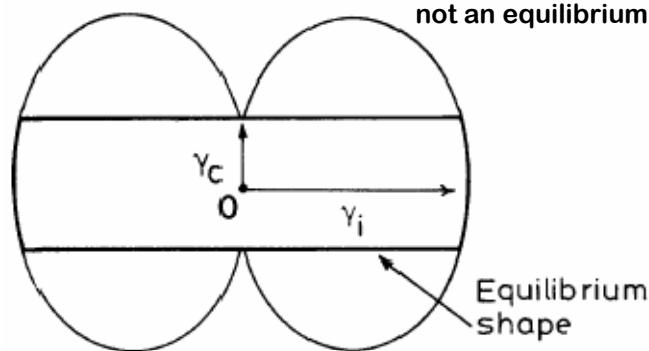


Fig. 3.40 A section through a γ -plot for a precipitate showing one coherent or semicoherent interface, together with the equilibrium shape (a disc).

Coherent or Semi-coherent in one Plane ; Disc Shape



hcp γ' Precipitates in Al – 4%Ag Alloys → plate broad face parallel to the $\{111\}_\alpha$ matrix planes

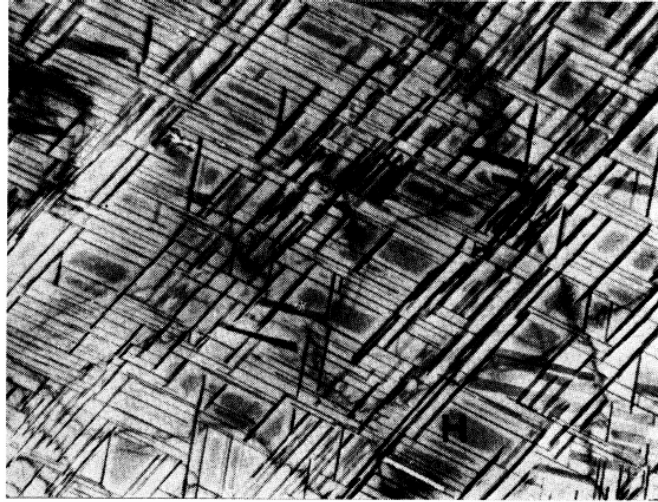


Fig. 3.42 Electron micrograph showing the Widmanstätten morphology of γ' precipitates in an Al-4 atomic % Ag alloy. GP zones can be seen between the γ' , e.g. at H ($\times 7000$). (R.B. Nicholson and J. Nutting, Acta Metallurgica, 9 (1961) 332.)

Phase



Precipitates on Grain Boundaries

- 1) incoherent interfaces with both grains
- 2) a coherent or semicoherent interface with one grain and an incoherent interface with the other,
- 3) coherent or semicoherent interface with both grains

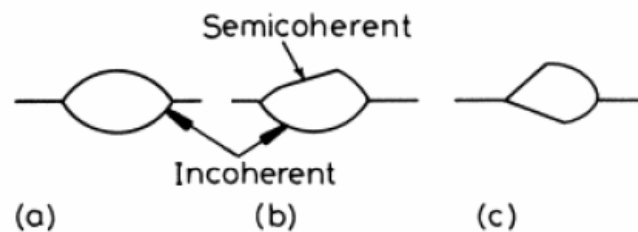


Fig. 3.45 Possible morphologies for grain boundary precipitates. Incoherent interfaces smoothly curved. Coherent or semicoherent interfaces planar.



Precipitates on Grain Boundaries

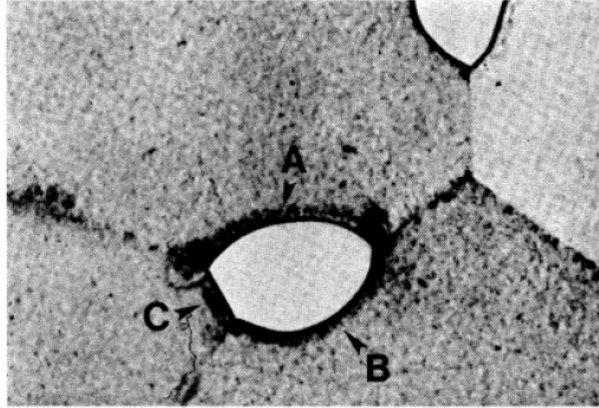


Fig. 3.46 An α precipitate at a grain boundary triple point in an $\alpha - \beta$ Cu-In alloy. Interfaces A and B are incoherent while C is semicoherent ($\times 310$). (After G.A. Chadwick, *Metallography of Phase Transformations*, Butterworths, London, 1972.)

A, B ; Incoherent
C ; Semicohherent



3.4.3. Second-Phase Shape: Misfit Strain Effects

$$\sum A_i \gamma_i + \Delta G_S = \text{minimum}$$

Fully Coherent Precipitates

Coherency Strain

Unconstrained Misfit

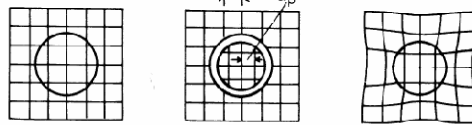
$$\delta = \frac{a_\beta - a_\alpha}{a_\alpha}$$

Constrained Misfit

$$\varepsilon = \frac{a'_\beta - a_\alpha}{a_\alpha}$$

$$\varepsilon = \frac{2}{3} \delta, \quad E_\beta = E_\alpha, \nu = 1/3$$

$$0.5\delta \leq \varepsilon \leq \delta, \quad E_\beta \neq E_\alpha$$



(a) (b) (c)
Fig. 3.47 The origin of coherency strains. The number of lattice points in the hole is conserved.

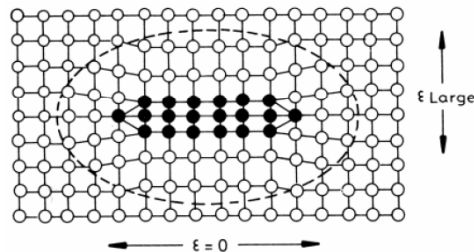


Fig. 3.48 For a coherent thin disc there is little misfit parallel to the plane of the disc. Maximum misfit is perpendicular to the disc.



Elastically Isotropic Materials
with equal elastic moduli
and $\nu = 1/3$

$$\Delta G_s = 4\mu\delta^2 \cdot V$$

μ : shear modulus of the matrix
 V : volume of the unconstrained hole

→ Independent of the shape of the precipitate

Different elastic moduli

→ Strain energy is minimum for a sphere for a hard inclusion

→ Strain energy is minimum for a disc for a soft inclusion

Elastically Anisotropic Materials

For most cubic metals, soft in $\langle 100 \rangle$ and hard in $\langle 111 \rangle$

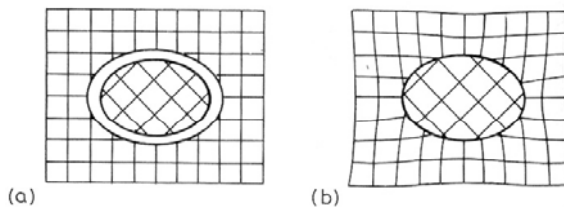
→ Disc parallel to $\{100\}$

Atom radius ($\overset{\circ}{\text{Å}}$)	Al : 1.43	Ag : 1.44	Zn : 1.38	Cu : 1.28
Zone Misfit (δ)	-	+ 0.7%	- 3.5%	- 10.5%
Zone Shape	-	sphere	sphere	disc



Incoherent Inclusions

$$\text{Volume Misfit } \Delta = \frac{\Delta V}{V}$$



For Elliptical Inclusions

$$\frac{x^2}{a^2} + \frac{y^2}{a^2} + \frac{z^2}{c^2} = 1$$

for a homogeneous
incompressible inclusion
in an isotropic matrix

$$\Delta G_s = \frac{2}{3} \mu \Delta^2 \cdot V \cdot f(c/a)$$

μ : the shear modulus of the matrix



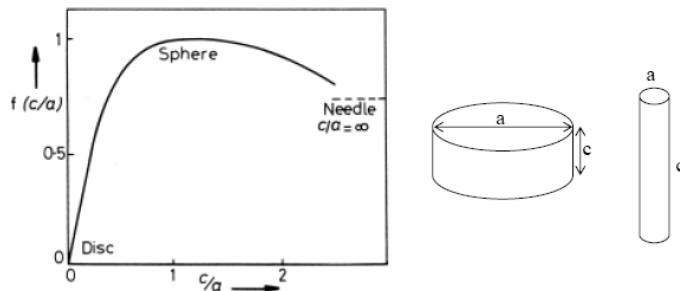


Fig. 3.50 The variation of misfit strain energy with ellipsoid shape, $f(c/a)$. (After F.R.N. Nabarro, *Proceedings of the Royal Society A*, 175 (1940) 519.)

$$\Delta G_s = \frac{2}{3} \mu \Delta^2 \cdot V \cdot f(c/a)$$

$$\Delta = \frac{V_\beta - V_\alpha}{V_\alpha} \approx 3\delta \text{ for sphere}$$

$$\neq 3\delta \text{ for disc or needle}$$



Coherency Loss

$$\Delta G(\text{coherent}) = 4\mu\delta^2 \cdot \frac{4}{3} \pi r^3 + 4\pi r^2 \cdot \gamma_{ch}$$

$$\Delta G(\text{non-coherent}) = 4\pi r^2 \cdot (\gamma_{ch} + \gamma_{st})$$

$$\frac{4}{3} \pi r^3 (4\pi\mu\delta^2) + 4\pi r^2 (\gamma_{ch}) = 4\pi r^2 (\gamma_{st} + \gamma_{ch})$$

coherent

ΔG_s -relaxed

$$\therefore r_{crit} = \frac{3 \cdot \gamma_{st}}{4\mu\delta^2}$$

$$\approx \frac{1}{\delta}$$

for small δ , $\gamma_{st} \propto \delta$

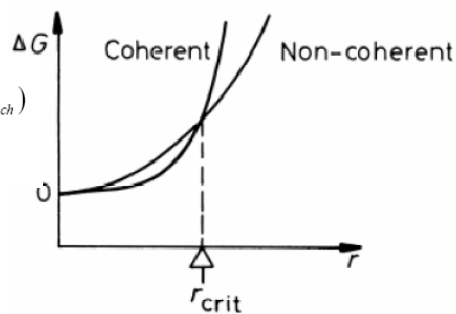


Fig. 3.52 The total energy of matrix + precipitate v. precipitate radius for spherical coherent and non-coherent (semicoherent or incoherent) precipitates.



Glissile Interfaces

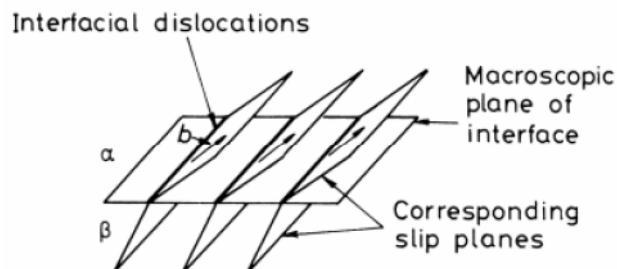
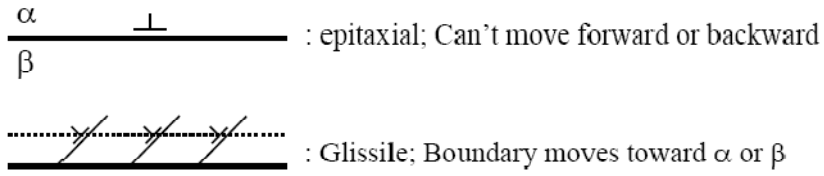


Fig. 3.55 The nature of a glissile interface.



Glissile Interfaces

HCP: ABABABAB...
 close packed plane: $\{0001\}$
 close packed directions:
 $\langle 11\bar{2}0 \rangle$

FCC: ABCABCAB...
 close packed planes: $\{111\}$
 close packed directions:
 $\langle 110 \rangle$

$B \rightarrow C$ sites

$$b = \frac{a}{6} \langle 11\bar{2} \rangle$$

\rightarrow Shockley partial dislocation

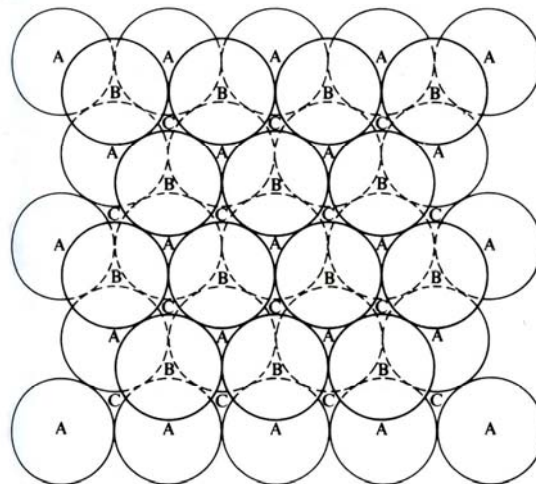


Fig. 3.56 The location of A, B and C sites in a close-packed layer of atoms. See also Figs. 3.57 and 3.58. (After J.W. Martin and R.D. Doherty, *Stability of Microstructure in Metallic Systems*, Cambridge University Press, Cambridge, 1976.)



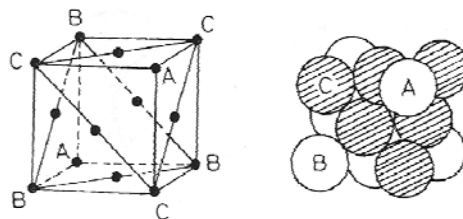


Fig. 3.58 A cubic close-packed structure showing fcc unit cell and stacking sequence.

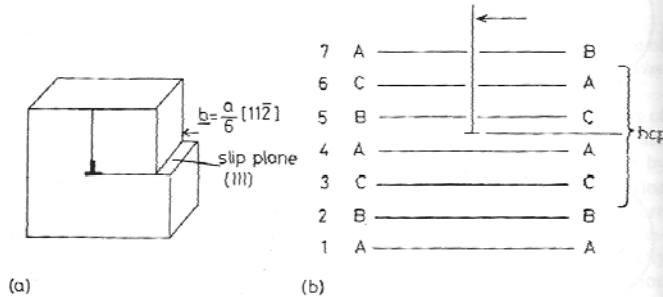


Fig. 3.59 (a) An edge dislocation with a Burgers vector $b = \frac{a}{6} [11\bar{2}]$ on (111). (Shockley partial dislocation.) (b) The same dislocation locally changes the stacking sequence from fcc to hcp.

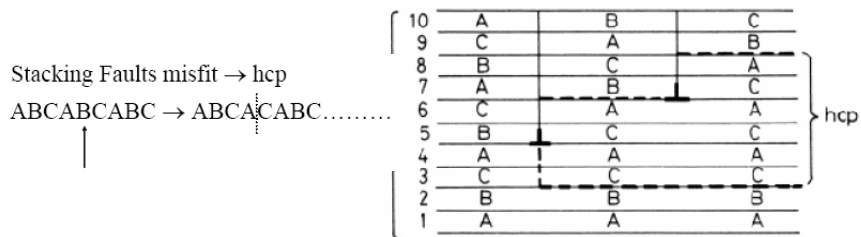


Fig. 3.60 Two Shockley partial dislocations on alternate (111) planes create six layers of hcp stacking.

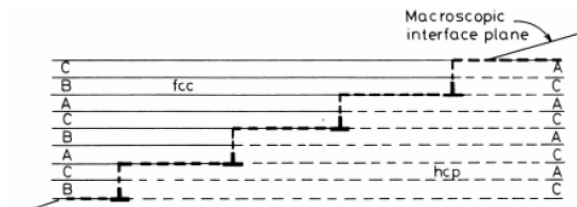
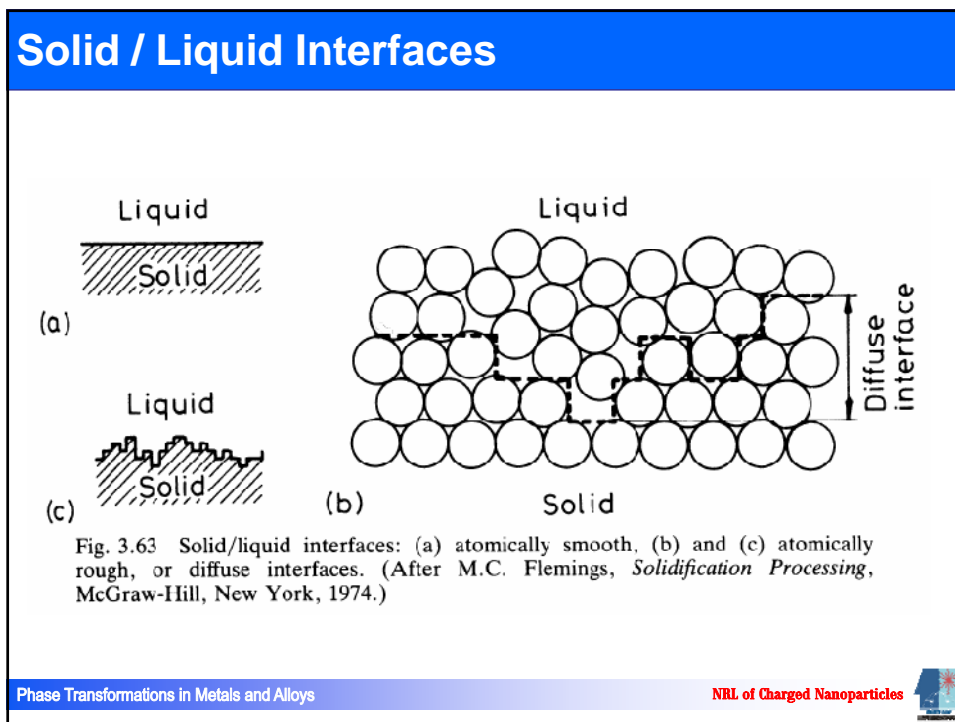
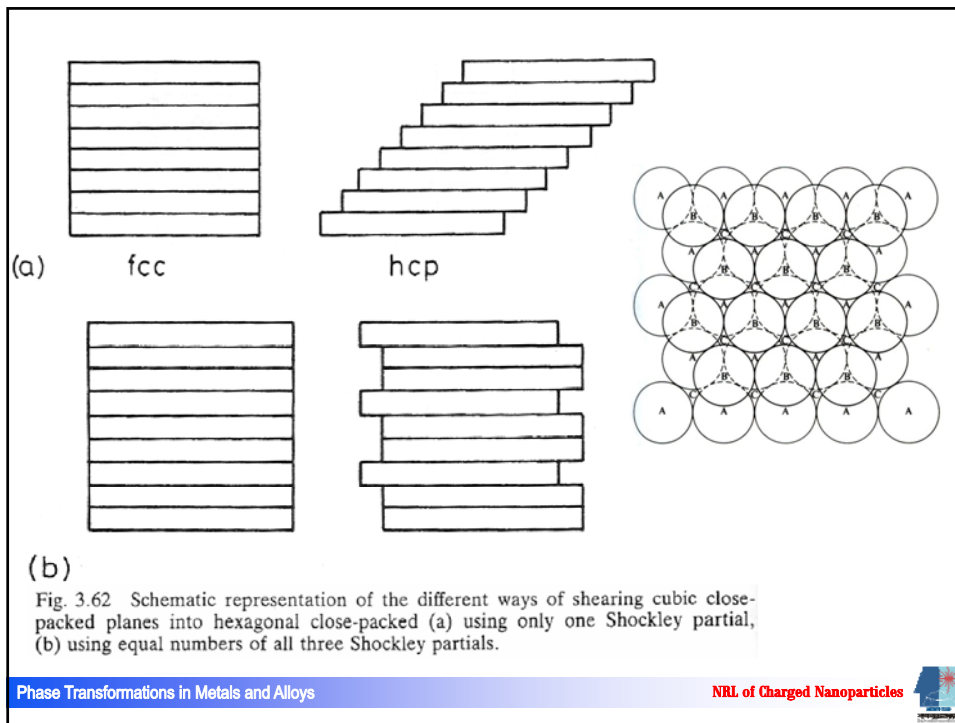
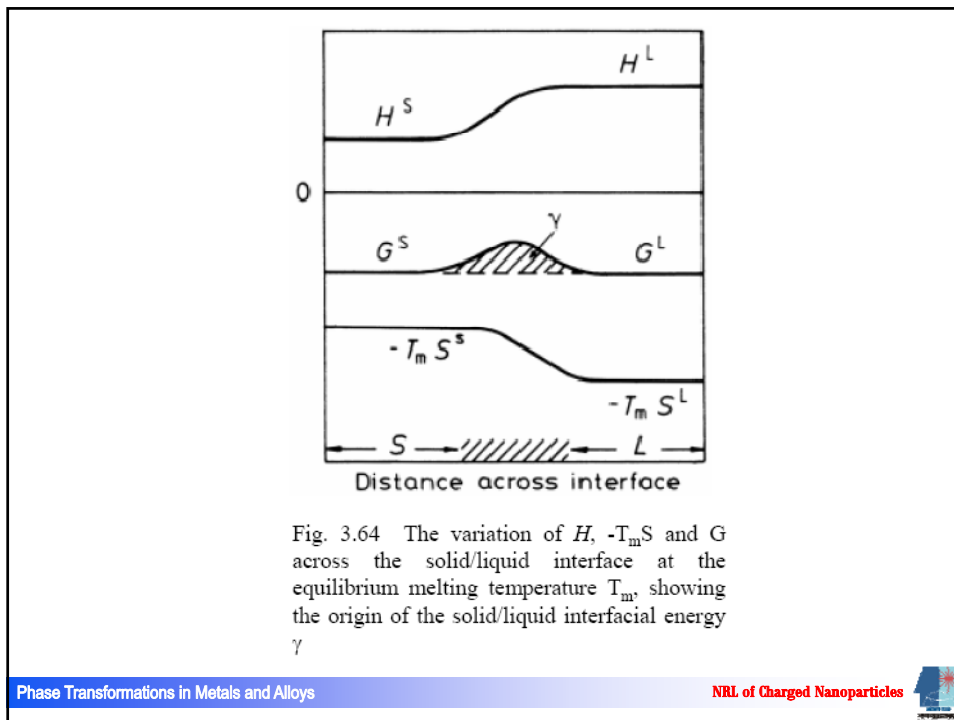


Fig. 3.61 An array of Shockley partial dislocations forming a glissile interface between fcc and hcp crystals.







Interface Migration

○ B
● A

Heterogeneous Transformation: Nucleation + Growth
Nucleation barrier
Eg. Precipitation

Homogeneous Transformation:
No nucleation barrier
Growth: Interface control
Eg. Spinodal

Types of Interface
- Glissile Interface: Military, Athermal: Shape change
- Non-Glissile Interface: Civilian, Thermal

Fig. 3.66 Composition changes in a substitutional alloy caused by interface migration when the two adjoining phases have different compositions.

Phase Transformations in Metals and Alloys NRL of Charged Nanoparticles

Diffusion-Controlled and Interface-Controlled Growth

$$\begin{aligned}
 J_B^i &= -C_B^i v_B \\
 &= -\frac{1}{V_m} (M \cdot \Delta\mu_B^i \cdot \frac{1}{V_m}) \qquad \Delta\mu_B^i \frac{1}{V_m} = \frac{J \text{ mol}^{-1}}{m^3 \text{ mol}^{-1}} \\
 &= J_B^\alpha = -D \left(\frac{\partial C_B}{\partial X} \right)_{\text{interface}}
 \end{aligned}$$

High Mobility: $\Delta\mu_B^i$ small, $X_i \approx X_e$, Diffusion-Control

Low Mobility: $\Delta\mu_B^i$ must be large, Mixed-Control

Very low Mobility: $X_i \approx X_0$, $\left(\frac{\partial C}{\partial X} \right)_{\text{interface}} \approx 0$, Interface-Control



Fig.3.67 *Interface migration with long – range diffusion. (a) Composition profiles across the interface. (b) The origin of the driving force for boundary migration into the α phase. (c) A schematic molar free energy diagram showing the relationship between $\Delta\mu_B^i$, X_i and X_e . (Note that the solubility of A in the β phase is so low that the true shape of the free energy curve cannot be drawn on this scale.*

